Available online at www.sciencedirect.com
ScienceDirect
Journal of Sound and Vibration 317 (2008) 739–759
JOURNAL OF SOUND AND VIBRATION
www.elsevier.com/locate/jsvi

Modal analysis of liquid sloshing with different contact line boundary conditions using FEM

Wang Wei, Li Junfeng, Wang Tianshu*

School of Aerospace, Tsinghua University, Beijing 100084, China

Received 5 March 2007; received in revised form 14 December 2007; accepted 30 March 2008
Handling Editor: L.G. Tham
Available online 10 June 2008

Abstract

A finite element method (FEM) for liquid sloshing modal analysis is established. Surface tension and three kinds of contact line boundary conditions, namely, free-end, pin-end and wetting boundary conditions, are taken into account. Sloshing damping caused by energy dissipation at the wall, in the interior fluid and at the contact line is calculated. Numerical results are compared with the analytical values and measurements. For the pin-end and free-end boundary conditions the differences between numerical value and analytical value are small, and for the wetting boundary condition, because approximation is used, the differences are more significant.

1. Introduction

The phenomenon of liquid sloshing in a rigid container has been studied for many years [1,2]. It is especially important for the stability of liquid-filled spacecrafts. In order to deal with the sloshing problem in low-gravity environments, the capillary effect has to be taken into account. It is well known that the behavior of the contact line plays an important role in determining the frequencies, damping rates, and waveforms of capillary-gravity waves, so a suitable contact line boundary condition is very necessary. The first contact line boundary condition adopted is free-end boundary condition. It assumes that the contact angle remains unchanged and the contact line can freely slip during sloshing. But the prediction with this boundary condition is not always consistent with the experiment results. In order to explain this discrepancy, Benjamin and Scott [3] and Graham-Eagle [4] made the assumption that under certain circumstances the contact line can remain at rest even in the presence of oscillation of the free surface. This boundary condition is known as the pinned-end boundary condition. The experiment of Henderson and Miles [5] showed it is the appropriate boundary condition for small amplitude liquid sloshing in a brimful container. When the container is not brimful and the sloshing is in a low-amplitude regime, the validity of the boundary condition was also confirmed experimentally by Cocciaro et al. [6]. But in cases when the container is not brimful and the sloshing is in a high amplitude regime, a more complex boundary condition has to be introduced. Hocking [7] and Miles

*Corresponding author. Tel.: +86 10 62773402.
E-mail address: tswang@mail.tsinghua.edu.cn (W. Tianshu).

0022-460X/$ - see front matter © 2008 Elsevier Ltd. All rights reserved.
doi:10.1016/j.jsv.2008.03.070

Nomenclature

$\mathbf{A}$	an $n_f \times n_f$ matrix
$\mathbf{A}'$	reduced matrix of $\mathbf{A}$
$\mathbf{B}$	an $n_f \times n_f$ matrix
$\mathbf{B}'$	reduced matrix of $\mathbf{B}$
$\mathbf{B}^i$	area element matrix in element i
$B_{jk}{}^i$	element of matrix $\mathbf{B}^{\mathbf{i}}$
$\mathbf{C}$	an $n_f \times n_f$ matrix
$\mathbf{C}'$	reduced matrix of $\mathbf{C}$
D_1	energy dissipation ratio in Stokes boundary layer
D_2	energy dissipation ratio in inner flow
$\mathbf{D}^i$	line element matrix in element i
$D_{jk}{}^i$	element of matrix $\mathbf{D}^i$
E	mean total energy
f	a specified function on S_f.
F	liquid dissipation function
g	effective gravitational acceleration
$\mathbf{G}$	an $n_f \times n_f$ matrix
h	amplitude of sloshing wave height
h_{ij}	value at node j in line element i
$\mathbf{h}^o$	a $n_f \times 1$ array
i	an integral number
j	an integral number
k	an integral number
$\mathbf{K}$	an $n_g \times n_g$ matrix
$\mathbf{K}_1$	an $n_f \times n_f$ matrix
$\mathbf{K}'_1$	an $(n_f-1) \times (n_f-1)$ matrix
$\mathbf{K}_2$	an $n_f \times (n_g-n_f)$ matrix
$\mathbf{K}'_2$	an $(n_f-1) \times (n_g-n_f)$ matrix
$\mathbf{K}_3$	an $(n_g-n_f) \times n_f$ matrix
$\mathbf{K}'_3$	an $(n_g-n_f) \times (n_f-1)$ matrix
$\mathbf{K}_4$	$(n_g-n_f) \times (n_g-n_f)$ matrix
$\mathbf{K}_5$	$n_f \times n_f$ matrix
$\mathbf{K}_5{}'$	an $n_f \times (n_f-1)$ matrix
$\mathbf{K}_5{}''$	an $n_f \times 1$ matrix
$\mathbf{K}_6$	an $(n_g-n_f) \times (n_f-1)$ matrix
$\mathbf{K}^i$	volume element matrix in element i
$K_{jk}{}^i$	element of matrix $\mathbf{K}^i$
l	number of nodes in area element
L	contact line
m	number of nodes in volume element
M_j	basis function of node j in area element
$\mathbf{n}$	interior normal unit vector at boundary
n_g	total number of all nodes
n_f	number of nodes at free surface
N_j	basis function of node j in volume element
p	number of nodes in line element
P_j	basis function of node j in line element
$\Re$	a function used in the expression of the dissipation function
r	number of nodal circles
s	number of nodal diameters
S_f	free surface
S_f^i	region of area element i
S_w	wetting boundary
t	time
T	surface tension
U	amplitude of liquid velocity
$\mathbf{V}$	velocity vector of liquid
$\bar{V}$	velocity of liquid in Stokes boundary layer
V_x	x component of $\mathbf{V}$
V_y	y component of $\mathbf{V}$
V_z	z component of $\mathbf{V}$
V_0	velocity obtained by irrotational flow theory at wall
v	kinematic viscosity
α	a factor of the penalty function
γ_1	damping rate in Stokes boundary layer
γ_2	damping rate in inner flow
ζ	sloshing wave height
θ	angle between $\mathbf{n}$ and z-axis
λ	capillary coefficient
μ	dynamic viscosity
Π_1	functional in the case of pin-end boundary condition
Π_2	functional in Neumann problem
Π_3	functional in the case of free-end boundary condition
Π_4	functional in the case of wetting boundary condition
ρ	the liquid density
Φ	velocity potential
ϕ	amplitude of velocity potential
$\phi_1{}''$	the first element of $\boldsymbol{\varphi}_1$
ϕ_i	value of ϕ in element i
ϕ_{ij}	value of ϕ at node j in element i
$\boldsymbol{\varphi}_1$	an $n_f \times 1$ array
$\boldsymbol{\varphi}_1{}'$	an $(n_g-n_f-1) \times 1$ array
$\boldsymbol{\varphi}_2$	an $(n_g-n_f) \times 1$ array
$\boldsymbol{\varphi}^i$	an $m \times 1$ array of element i
$\boldsymbol{\varphi}_1^i$	an $l \times 1$ array of element i
$\boldsymbol{\varphi}^0$	an $n_g \times 1$ array
$\boldsymbol{\varphi}_1^0$	an $n_f \times 1$ array
$\aleph$	a function used in the dissipation function
ψ	phase difference between Φ and ζ
$<$	a temporary variable
ψ_1	phase difference between Φ and ζ

Ω	region of liquid	ω	sloshing frequency
Ω_i	region of volume element i	ω_1	complex frequency

[8,9] proposed a new and more general boundary condition where the contact angle is assumed to be a linear function of the contact line velocity. It is known as the 'wetting' boundary condition and contains the free-end and pinned-end boundary conditions as its limiting cases. In the experiment of Cocciaro et al. [6] a nonlinear dependence of the eigenfrequency and damping rate upon the oscillation amplitude is found in high amplitude regimes, and all the experimental results can be explained in terms of the wetting boundary condition, in which an 'effective' capillary coefficient is introduced.

Analytical methods for sloshing modal analysis usually make the assumption that the free surface is flat and the shape of the container holding the liquid is regular and simple, such as rectangular or cylindrical. But in a low-gravity environment the free surface is usually not flat. And in practice the shape of the container generally depends upon certain factors such as the design and environment, a wide variety of shapes, regular and irregular, are in use. It is therefore desirable to develop a numerical method to analyze the sloshing behavior of liquid in containers of a fairly general shape. General purpose computational fluid dynamics (CFD) codes with a free surface capability can be used to analyze the small amplitude sloshing of liquid with capillary effect directly. But CFD codes always call for relatively large computing resources and have difficulty in calculating the damping rate. There are two difficulties. First, the numerical dissipation will influence the damping rate computation and make the numerical results undependable. Second, the computing of dissipation near the wall and the free surface required refined grids and causes the computational quantity to increase dramatically. So modal analysis other than direct CFD simulation is a more effective way to obtain the frequencies and damping rates of sloshing. To the best of our knowledge, the Ritz method is the only numerical method that has been used for the modal analysis of the small amplitude sloshing of liquid with capillary effect. However, it depends on the shape of the liquid field and is not convenient to use. In the present paper, finite element method (FEM) is employed to deal with this problem, and recent advances in contact line boundary condition and damping rate computation are taken into account.

2. Theory

In the case of liquid sloshing with small amplitude, viscosity only seriously influences the flow in a thin layer near the rigid boundary, which is called the Stokes boundary layer. The flow outside this boundary layer can be considered as an irrotational flow. So the theoretical model of liquid sloshing with small amplitude is divided into two parts: the Stokes boundary layer at the rigid boundary and the irrotational flow outside the boundary layer. The eigenfrequencies and modes of sloshing will be calculated by the irrotational flow theory, and the damping will be calculated in both the irrotational flow and the Stokes boundary layer.

2.1. Irrotational flow theory

As shown in Fig. 1, Ω denotes the region of the liquid, S_w the wetting boundary, S_f the free surface, L the contact line, $\mathbf{n}$ the interior normal unit vector at the boundary, ζ the sloshing wave height measured in the $\mathbf{n}$ direction, T the surface tension, ρ the liquid density, and g the effective gravitational acceleration. A Cartesian reference frame $oxyz$ is defined with z measured in the direction opposite to gravitational acceleration. Generally speaking, the thickness of the Stokes boundary layer is very small, so the rigid boundary of the irrotational flow can be approximately replaced by the wetting boundary S_w. Designating the velocity of liquid as $\mathbf{V}$ and the velocity potential as Φ; then

$$\mathbf{V} = \nabla\Phi. \tag{1}$$

The irrotational flow problem is prescribed by

$$\nabla^2\Phi = 0 \ \ (\text{in } \Omega), \tag{2}$$

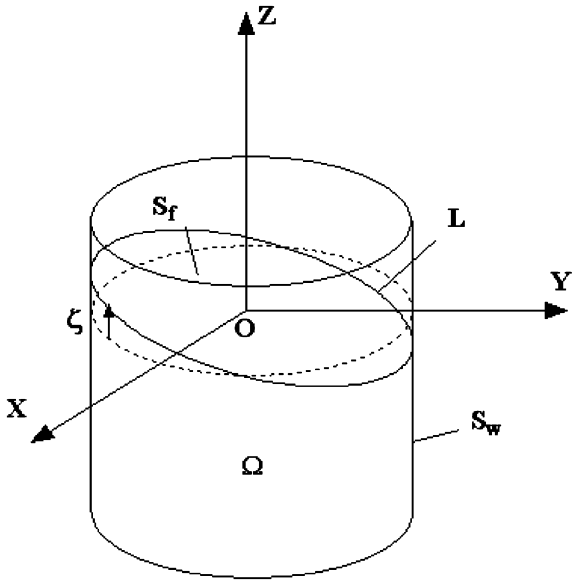

Fig. 1. Sketch map of liquid sloshing problem in rigid container.

$$\frac{\partial \Phi}{\partial \mathbf{n}} = 0 \text{ (on } S_w), \tag{3}$$

$$\frac{\partial \Phi}{\partial t} - \left(\frac{g}{\cos\theta} - \frac{T}{\rho}\nabla^2\right)\zeta = 0 \text{ (on } S_f), \tag{4}$$

$$\frac{\partial \Phi}{\partial \mathbf{n}} = \frac{\partial \zeta}{\partial t} \text{ (on } S_f), \tag{5}$$

where θ is the angle between between $\mathbf{n}$ and the z-axis. In the present paper three kinds of contact line boundary conditions will be considered: they are the free-end boundary condition

$$\frac{\partial \zeta}{\partial \mathbf{n}} = 0 \text{ (on } L) \tag{6}$$

the pin-end boundary condition

$$\zeta = 0 \text{ (on } L) \tag{7}$$

and the wetting boundary condition

$$\frac{\partial \zeta}{\partial t} = \lambda \frac{\partial \zeta}{\partial \mathbf{n}} \text{ (on } L), \tag{8}$$

where λ is the phenomenological capillary coefficient, which was proposed by Hocking [7] and Miles [8,9]. An important feature of the wetting boundary condition is that it includes, as special cases, both the free-end ($\lambda = \infty$) and the pinned-end ($\lambda = 0$) boundary conditions.

2.2. Damping calculation

The theoretical analysis of damping in liquid sloshing with small amplitude goes back to Stokes (1851). He calculated the flow over an oscillating plane, and remarked that the corresponding flow over an oscillating curved boundary may be calculated to a very close degree of approximation by regarding each element of the boundary as an infinite plane oscillating with the same velocity. But there is large difference between the predicted value using this method and the measured value. It is pointed out in Ref. [6] that the damping of liquid sloshing is due to: (i) viscous dissipation at the rigid boundary of the container, (ii) viscous dissipation at

the free surface, which may be covered by a viscoelastic film, (iii) viscous damping in the interior fluid, and (iv) capillary hysteresis at the contact line. If the free surface is clean, (ii) does not exist and will not be considered in the present paper. The Stokes boundary layer theory is used to calculate the dissipation at the rigid boundary, so it will be introduced here. Usually the thickness of the Stokes boundary layer is very small, so the wall can be treated as an infinite plane when studying the flow near the wall. As shown in Fig. 2, in the Stokes boundary layer the velocity of liquid is approximately parallel to the wall, the flow is prescribed by

$$\frac{\partial \bar{V}}{\partial t} = v\frac{\partial^2 \bar{V}}{\partial z^2}, \tag{9}$$

where $\bar{V}$ is velocity of liquid in the Stokes boundary layer, z is the normal coordinate of the wall, and v is the kinematic viscosity. The boundary condition at the wall is

$$\bar{V} = 0 \ (z = 0). \tag{10}$$

At the outside boundary of the Stokes boundary layer, $\bar{V}$ can be replaced by V_0, which is the velocity obtained by the irrotational flow theory:

$$\bar{V} = V_0 \ (z \to \infty). \tag{11}$$

In the case of free oscillation, V_0 can be expressed as $V_0 = U\mathrm{e}^{\mathrm{i}\omega t}$, where ω is the sloshing frequency, and U is the amplitude. From the equation and boundary conditions above, we can obtain

$$\bar{V} = U\mathrm{e}^{\mathrm{i}\omega t}\{1 - \exp[-(\mathrm{i}\omega/v)^{1/2}z]\}. \tag{12}$$

The mean energy dissipation ratio in the Stokes boundary layer in a sloshing period is

$$D_1 = \frac{1}{2}\rho\left(\frac{1}{2}v\omega\right)^{1/2}\iint_{S_w}|U|^2\,\mathrm{d}S. \tag{13}$$

For free oscillation, Φ can be written as

$$\Phi = \phi\sin\omega t, \tag{14}$$

where ϕ is amplitude. Then the mean total energy is

$$E = \frac{\rho}{2}\int_{\Omega}|\nabla\phi|^2\,\mathrm{d}\Omega. \tag{15}$$

The damping rate at the rigid boundary is

$$\gamma_1 = \frac{D_1}{2\omega E}. \tag{16}$$

The damping rate in the inner fluid will be calculated next. The dissipation function for viscous dissipation of liquid is

$$F = \frac{\mu}{2}\int_{\Omega}\aleph(\mathbf{V})\,\mathrm{d}\Omega, \tag{17}$$

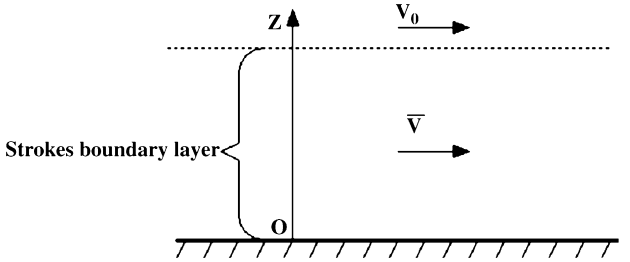

Fig. 2. Sketch map of Stokes boundary layer.

where

$$\mathbf{V} = [V_x \quad V_y \quad V_z]^{\mathrm{T}},$$

$$\aleph(\mathbf{V}) = 2\left(\frac{\partial V_x}{\partial x}\right)^2 + 2\left(\frac{\partial V_y}{\partial y}\right)^2 + 2\left(\frac{\partial V_z}{\partial z}\right)^2 + \left(\frac{\partial V_z}{\partial y} - \frac{\partial V_y}{\partial z}\right)^2 + \left(\frac{\partial V_x}{\partial z} - \frac{\partial V_z}{\partial x}\right)^2 + \left(\frac{\partial V_y}{\partial x} - \frac{\partial V_x}{\partial y}\right)^2$$

and μ is the dynamic viscosity. The inner flow is simulated according to the irrotational flow theory. Strictly speaking, there is no dissipation for an irrotational flow, but the dissipation function of an irrotational flow could be written as an approximation. Using $\mathbf{V} = \nabla\Phi$, Eq. (17) can be expressed as

$$F = \frac{\mu}{2}\int_{\Omega} \Re(\Phi)\,\mathrm{d}\Omega, \tag{18}$$

where

$$\Re(\Phi) = 2\left(\frac{\partial^2\Phi}{\partial x^2}\right)^2 + 2\left(\frac{\partial^2\Phi}{\partial y^2}\right)^2 + 2\left(\frac{\partial^2\Phi}{\partial z^2}\right)^2 + 4\left(\frac{\partial^2\Phi}{\partial x\,\partial y}\right)^2 + 4\left(\frac{\partial^2\Phi}{\partial y\,\partial z}\right)^2 + 4\left(\frac{\partial^2\Phi}{\partial z\,\partial x}\right)^2.$$

Then in the case of free oscillation the mean energy dissipation ratio for the inner flow in a sloshing period is obtained approximately as

$$D_2 = \frac{\omega}{2\pi}\int_0^{2\pi/\omega} 2F\,\mathrm{d}t = \frac{\omega}{2\pi}\int_0^{2\pi/\omega} \mu\int_{\Omega} \Re(\phi)\,\mathrm{d}\Omega\cos^2\omega t\,\mathrm{d}t = \frac{1}{2}\mu\int_{\Omega} \Re(\phi)\,\mathrm{d}\Omega \tag{19}$$

and the damping rate in the inner flow is

$$\gamma_2 = \frac{D_2}{2\omega E} \tag{20}$$

In the case of free-end and pin-end boundary conditions, there is no dissipation at the contact line, and in the case of the wetting boundary condition, if $\lambda \neq 0$, the movement of contact line will cause dissipation. When the irrotational flow theory and wetting boundary condition are used in the modal analysis of liquid sloshing, the results of frequencies will be complex numbers whose real parts are minus and denote damping rates caused by the dissipation at the contact line. The details of this will be described later.

3. Modal analysis in FEM

For different contact line boundary conditions, the FEMs used for the modal analysis of liquid sloshing are somewhat different. So the three kinds of contact line boundary conditions will be dealt with separately.

3.1. Pin-end boundary condition

In the case of an irrotational flow and pin-end boundary condition there is no dissipation during sloshing, so Φ and ζ in free oscillation can be expressed as

$$\Phi = \phi\sin\omega t, \tag{21a}$$

$$\zeta = h\sin(\omega t + \psi), \tag{21b}$$

where ϕ and h denote amplitude and ψ denotes the phase difference between Φ and ζ. Substituting Eq. (21a, b) into Eq. (5), we can obtain

$$\frac{\partial\phi}{\partial\mathbf{n}}\sin\omega t = \omega h\cos(\omega t + \psi). \tag{22}$$

In order to make the equation above valid, ψ must have the form of

$$\psi = (k + 1/2)\pi. \tag{23}$$

Let $\psi = \pi/2$, Eq. (21) can be rewritten as

$$\Phi = \phi \sin \omega t, \tag{24a}$$

$$\zeta = h \cos \omega t. \tag{24b}$$

Substituting Eq. (24) into Eqs. (2), (3), (4), (5), (7), we can obtain the equation and boundary conditions that only contain the space variables

$$\nabla^2 \phi = 0 \text{ in } \Omega \tag{25}$$

$$\frac{\partial \phi}{\partial \mathbf{n}} = 0 \text{ on } S_w \tag{26}$$

$$h\omega = \frac{\partial \phi}{\partial \mathbf{n}} \text{ on } S_f \tag{27}$$

$$\omega\phi - \left(\frac{a}{\cos\theta} - \frac{T}{\rho}\nabla^2\right)h = 0 \text{ on } S_f \tag{28}$$

$$h = 0 \text{ on } L. \tag{29}$$

3.1.1. FEM dispersion

In order to use FEM, variational formulation of liquid sloshing has to be established first. The Galerkin statement of equivalent weak formulation of the Eq. (25) and boundary conditions (26) and (28) is

$$\int_\Omega \nabla^2\phi\delta\phi \,\mathrm{d}\Omega - \int_{S_w} \frac{\partial\phi}{\partial\mathbf{n}}\delta\phi \,\mathrm{d}S - \int_{S_f}\left(\left(\frac{a}{\cos\theta} - \frac{T}{\rho}\nabla^2\right)h - \omega\phi\right)\delta h \,\mathrm{d}S = 0. \tag{30}$$

Using integration by parts we can get the equations

$$\int_\Omega \nabla^2\phi\delta\phi \,\mathrm{d}\Omega = \frac{1}{2}\delta\left(-\int_\Omega \nabla\phi\,\nabla\phi \,\mathrm{d}\Omega\right) + \int_{S_w+S_f} \delta\phi \frac{\partial\phi}{\partial\mathbf{n}} \,\mathrm{d}S \tag{31}$$

and

$$\int_{S_f} \nabla^2 h\delta h \,\mathrm{d}S = \oint_L \frac{\partial h}{\partial\mathbf{n}}\delta h \,\mathrm{d}L - \int_{S_f} \nabla(h)\nabla\delta h \,\mathrm{d}S = -\int_{S_f} \nabla h\delta\nabla h \,\mathrm{d}S \tag{32}$$

Eq. (29) is used to make the second equation of Eq. (32) valid. Substituting Eqs. (31) and (32) into Eq. (30) and using Eq. (27), we can obtain the variational formulation

$$\delta\Pi_1 = 0, \tag{33}$$

where

$$\Pi_1 = \int_\Omega \nabla\phi\,\nabla\phi \,\mathrm{d}\Omega - \int_{S_f} \frac{a}{\cos\theta} h^2 \,\mathrm{d}S - \int_{S_f} \frac{T}{\rho}\nabla h\nabla h \,\mathrm{d}S. \tag{34}$$

The pin-end boundary condition (29) is a coercive boundary condition, so it has to be applied in the variational formulation above. There are two ways for it to be applied. One is to let the wave height at the contact line be zero directly; the other is the penalty function method, namely

$$\Pi_1 = \int_\Omega \nabla\phi\nabla\phi \,\mathrm{d}\Omega - \int_{S_f} \frac{a}{\cos\theta} h^2 \,\mathrm{d}S - \int_{S_f} \frac{T}{\rho}\nabla h\nabla h \,\mathrm{d}S - \alpha\int_L h^2 \,\mathrm{d}L, \tag{35}$$

where α is a constant whose value should be selected properly. When α is too small, the penalty function will lose its effect, and when α is too large, the matrix in the FEM will be ill-conditioned.

In variational formulation (34) there are two kinds of variables, the velocity potential ϕ and the wave height. Eq. (27) means that h can be expressed in terms of $\partial\phi/\partial\mathbf{n}$ at the free surface. On the other hand, according to the Neumann problem of the Laplace equation, ϕ in Ω can be determined by $\partial\phi/\partial\mathbf{n}$ at S_f and S_w. At S_w $\partial\phi/\partial\mathbf{n}=0$, then ϕ in Ω can be determined by $\partial\phi/\partial\mathbf{n}$ at S_f. So $\partial\phi/\partial\mathbf{n}$ at S_f will be selected as the variable of FEM modal analysis. In order to establish the relationship between ϕ in Ω and $\partial\phi/\partial\mathbf{n}$ at S_f, the variational formulation of the Neumann problem needs to be used. The Neumann problem can be expressed as

$$\nabla^2\phi = 0, \tag{36}$$

$$\frac{\partial\phi}{\partial\mathbf{n}} = 0 \ (\text{on } S_w), \tag{37}$$

$$\frac{\partial\phi}{\partial\mathbf{n}} = f \ (\text{on } S_f), \tag{38}$$

where f is a specified function on S_f. The Galerkin statement of equivalent weak formulation of the equation and boundary conditions above is

$$\int_\Omega \nabla^2\phi\delta\phi \,\mathrm{d}\Omega - \int_{S_w} \frac{\partial\phi}{\partial\mathbf{n}}\delta\phi \,\mathrm{d}S - \int_{S_f}\left(\frac{\partial\phi}{\partial\mathbf{n}} - f\right)\delta\phi \,\mathrm{d}S = 0. \tag{39}$$

Using Eq. (31), we can obtain the variational formulation

$$\delta\Pi_2 = 0, \tag{40}$$

where

$$\Pi_2 = \int_\Omega \nabla\phi\nabla\phi \,\mathrm{d}\Omega - \int_{S_f} \phi\frac{\partial\phi}{\partial n} \,\mathrm{d}S. \tag{41}$$

The finite element dispersion is carried out on the basis of the variational formulations (33) and (40). The relationship of ϕ in Ω and $\partial\phi/\partial\mathbf{n}$ at S_f is established in discrete form first. Let every volume element have m nodes. In volume element i, ϕ is expressed as

$$\phi_i = \sum_{j=1}^{m} \phi_{ij} N_j, \tag{42}$$

where ϕ_{ij} is the value at node j in volume element i, and N_j is the basis function of node j. Let every area element have l nodes. In area element i, ϕ and $\partial\phi/\partial\mathbf{n}$ are expressed as

$$\phi_i = \sum_{j=1}^{l} \phi_{ij} M_j, \tag{43}$$

$$\left(\frac{\partial\phi}{\partial\mathbf{n}}\right)_i = \sum_{j=1}^{l} \left(\frac{\partial\phi}{\partial\mathbf{n}}\right)_{ij} M_j, \tag{44}$$

where ϕ_{ij} and $(\partial\phi/\partial\mathbf{n})_{ij}$ are the values at node j in area element i, and M_j is the basis function of node j. Substituting Eqs. (42), (43), and (44) into Eq. (41), we can obtain the discrete representation of Eq. (41):

$$\Pi_2 = \sum_i \sum_{j=1}^{m}\sum_{k=1}^{m} \phi_{ij}\left(\int_{\Omega_i} \nabla N_j \nabla N_k \,\mathrm{d}\Omega_i\right)\phi_{ik} - \sum_i \sum_{j=1}^{l}\sum_{k=1}^{l} \phi_{ij}\left(\int_{s_f^i} M_j M_k \,\mathrm{d}S_i\right)\left(\frac{\partial\phi}{\partial\mathbf{n}}\right)_{ik}, \tag{45}$$

where Ω_i is the region of volume element i, and S_f^i is the region of area element i. Π_2 can be further expressed as

$$\Pi_2 = \sum_i \boldsymbol{\varphi}^{i\mathrm{T}}\mathbf{K}^i\boldsymbol{\varphi}^i - \sum_i \boldsymbol{\varphi}_1^{i\mathrm{T}}\mathbf{B}^i\left(\frac{\partial\phi}{\partial\mathbf{n}}\right)^i, \tag{46}$$

where

$$\boldsymbol{\varphi}^i = [\phi_{i1}, \phi_{i2} \dots \phi_{im}]^{\mathrm{T}}$$

$$\boldsymbol{\varphi}_1^i = [\phi_{i1}, \phi_{i2} \dots \phi_{il}]^{\mathrm{T}}$$

$$\left(\frac{\partial \phi}{\partial \mathbf{n}}\right)^i = \left[\left(\frac{\partial \phi}{\partial \mathbf{n}}\right)_{i1}, \left(\frac{\partial \phi}{\partial \mathbf{n}}\right)_{i2} \cdots \left(\frac{\partial \phi_{il}}{\partial \mathbf{n}}\right)_{i2}\right]^{\mathrm{T}}$$

$$\mathbf{K^i} = \{K_{jk}^i\}, \quad K_{jk}^i = \int_{\Omega_i} \nabla N_j \nabla N_k \, \mathrm{d}\Omega_i, \quad j,k = 1,2,\dots,m,$$

$$\mathbf{B^i} = \{B_{jk}^i\}, \quad B_{jk}^i = \int_{s_f^i} M_j M_k \, \mathrm{d}S_i, \quad j,k = 1,2,\dots,l.$$

The values of ϕ at all nodes are arranged as a column matrix $\boldsymbol{\varphi}^{\mathrm{o}}$ of order n_g where n_g is the number of all nodes. Let the nodes at the free surface be arranged into the first n_f positions of $\boldsymbol{\varphi}^o$ where n_f is the number of nodes at the free surface. $\boldsymbol{\varphi}_1^o$ is a column matrix of order n_f corresponding to the first n_f elements of $\boldsymbol{\varphi}^{\mathrm{o}}$. The values of $\partial\phi/\partial\mathbf{n}$ at all free surface nodes are arranged as a column matrix $(\partial\phi/\partial\mathbf{n})^o$, and then

$$\Pi_2 = \boldsymbol{\varphi}^{o\mathrm{T}} \mathbf{K} \boldsymbol{\varphi}^o - \boldsymbol{\varphi}_1^{o\mathrm{T}} \mathbf{B} \left(\frac{\partial \phi}{\partial \mathbf{n}}\right)^o, \tag{47}$$

where $\mathbf{K}$ and $\mathbf{B}$ are assembled from $\mathbf{K}^i$ and $\mathbf{B}^i$. $\mathbf{K}$ is a matrix of size $n_g \times n_g$, and $\mathbf{B}$ is a matrix of size $n_f \times n_f$.

The matrixes $\mathbf{K}$ and $\boldsymbol{\varphi}^o$ are divided as follows:

$$\mathbf{K} = \begin{bmatrix} \mathbf{K}_1 & \mathbf{K}_2 \\ \mathbf{K}_3 & \mathbf{K}_4 \end{bmatrix}, \quad \boldsymbol{\varphi}^o = \begin{bmatrix} \boldsymbol{\varphi}_1 \\ \boldsymbol{\varphi}_2 \end{bmatrix}, \tag{48}$$

where $\mathbf{K}_1$ is a matrix of size $n_f \times n_f$, $\mathbf{K}_2$ is a matrix of size $n_f \times (n_g - n_f)$, $\mathbf{K}_3$ is a matrix of size$(n_g - n_f) \times n_f$, $\mathbf{K}_4$ is a matrix of size $(n_g - n_f) \times (n_g - n_f)$, $\boldsymbol{\varphi}_1$ is an array of size $n_f \times 1$, and $\boldsymbol{\varphi}_2$ is an array of size $(n_g - n_f) \times 1$. Substituting Eqs. (47) and (48) into Eq. (40), we can obtain

$$\mathbf{K}_1\boldsymbol{\varphi}_1 + \mathbf{K}_2\boldsymbol{\varphi}_2 = \mathbf{B}\left(\frac{\partial \phi}{\partial \mathbf{n}}\right)^o, \tag{49}$$

$$\mathbf{K}_3\boldsymbol{\varphi}_1 + \mathbf{K}_4\boldsymbol{\varphi}_2 = 0. \tag{50}$$

Then $\boldsymbol{\varphi}_2$ and $(\partial\phi/\partial\mathbf{n})^o$ can be expressed in terms of $\boldsymbol{\varphi}_1$

$$\boldsymbol{\varphi}_2 = -\mathbf{K}_4^{-1}\mathbf{K}_3\boldsymbol{\varphi}_1, \tag{51}$$

$$\left(\frac{\partial \phi}{\partial \mathbf{n}}\right)^o = \mathbf{K}_5\boldsymbol{\varphi}_1, \tag{52}$$

where

$$\mathbf{K}_5 = \mathbf{B}^{-1}(\mathbf{K_1} - \mathbf{K}_2\mathbf{K}_4^{-1}\mathbf{K}_3). \tag{53}$$

Take notice of the fact that if a constant is added to the solution of Eqs. (36), (37), and (38), the result is still a solution. In order to eliminate this indeterminacy, the first element of $\boldsymbol{\varphi}_1$ is appointed to be zero. Let $\mathbf{K'}_5$ be a matrix of size $n_f \times (n_f - 1)$ that results from eliminating the first column of $\mathbf{K}_5$, and let $\boldsymbol{\varphi}_1'$ be an array of size $(n_f - 1) \times 1$ that results from eliminating the first element of $\boldsymbol{\varphi}_1$; then

$$\boldsymbol{\varphi}_1' = \mathbf{K'}_5^{+}\left(\frac{\partial \phi}{\partial \mathbf{n}}\right)^o, \tag{54}$$

where $\mathbf{K}'^{+}_{5}$ is the general inverse of $\mathbf{K}'_{5}$:

$$\mathbf{K}'^{+}_{5} = (\mathbf{K}'^{\mathrm{T}}_{5}\mathbf{K}'_{5})^{-1}\mathbf{K}'^{\mathrm{T}}_{5}. \tag{55}$$

The proof of Eq. (54) is as follows. The matrixes $\mathbf{K}_5$ and $\boldsymbol{\varphi}_1$ are divided as follows:

$$\mathbf{K}_5 = [\mathbf{K}''_5, \mathbf{K}'_5], \quad \boldsymbol{\varphi}_1 = \begin{bmatrix} \phi''_1 \\ \boldsymbol{\varphi}'_1 \end{bmatrix}. \tag{56}$$

Substituting Eq. (56) into Eq. (52), we can obtain

$$\mathbf{K}'_5\boldsymbol{\varphi}'_1 = \left(\frac{\partial\phi}{\partial\mathbf{n}}\right)^{o} - \mathbf{K}''_5\phi''_1. \tag{57}$$

Multiply the two sides of Eq. (57) by $\mathbf{K}'^{\mathrm{T}}_{5}$:

$$\mathbf{K}'^{\mathrm{T}}_{5}\mathbf{K}'_5\boldsymbol{\varphi}'_1 = \mathbf{K}'^{\mathrm{T}}_{5}\left(\frac{\partial\phi}{\partial\mathbf{n}}\right)^{o} - \mathbf{K}'^{\mathrm{T}}_{5}\mathbf{K}''_5\phi''_1. \tag{58}$$

Let $\phi_1'' = 0$; then

$$\mathbf{K}''^{\mathrm{T}}_{5}\mathbf{K}''_5\boldsymbol{\varphi}'_{\mathbf{1}} = \mathbf{K}'^{\mathrm{T}}_{5}\left(\frac{\partial\phi}{\partial\mathbf{n}}\right)^{o}. \tag{59}$$

Multiplying the two sides of Eq. (59) by $(\mathbf{K}'^{\mathrm{T}}_{5}\mathbf{K}'_5)^{-1}$, we can obtain Eq. (54). Let $\mathbf{K}_6$ be a matrix of size $(n_g{-}n_f)\times(n_f{-}1)$ that results from eliminating the first column of $\mathbf{K}_4^{-1}\mathbf{K}_3$; then

$$\boldsymbol{\varphi}_2 = -\mathbf{K}_6\boldsymbol{\varphi}'_1 = -\mathbf{K}_6\mathbf{K}'^{+}_{5}\left(\frac{\partial\phi}{\partial\mathbf{n}}\right)^{o}. \tag{60}$$

Eq. (60) establishes the relationship between ϕ and $\partial\phi/\partial\mathbf{n}$. Dispersing the viariational formulation (34) in the same way and using Eq. (27), we can obtain

$$\Pi_1 = \boldsymbol{\varphi}^{o\mathrm{T}}\mathbf{K}\boldsymbol{\varphi}^{o} - \frac{a}{\omega^2}\left(\frac{\partial\phi}{\partial\mathbf{n}}\right)^{o\mathrm{T}}\mathbf{B}\left(\frac{\partial\phi}{\partial\mathbf{n}}\right)^{o} - \frac{T}{\omega^2\rho}\left(\frac{\partial\phi}{\partial\mathbf{n}}\right)^{o\mathrm{T}}\mathbf{C}\left(\frac{\partial\phi}{\partial\mathbf{n}}\right)^{o}, \tag{61}$$

where $\mathbf{B}$ and $\mathbf{C}$ are matrices of size $n_f\times n_f$. In terms of Eq. (48), Π_1 can be written as

$$\Pi_1 = \boldsymbol{\varphi}_1^{\mathrm{T}}\mathbf{K}_1\boldsymbol{\varphi}_1 + \boldsymbol{\varphi}_1^{\mathrm{T}}\mathbf{K}_2\boldsymbol{\varphi}_2 + \boldsymbol{\varphi}_2^{\mathrm{T}}\mathbf{K}_3\boldsymbol{\varphi}_1 + \boldsymbol{\varphi}_2^{\mathrm{T}}\mathbf{K}_4\boldsymbol{\varphi}_2 - \frac{1}{\omega^2}\left(\frac{\partial\phi}{\partial\mathbf{n}}\right)^{o\mathrm{T}}\left(a\mathbf{B}+\frac{T}{\rho}\mathbf{C}\right)\left(\frac{\partial\phi}{\partial\mathbf{n}}\right)^{o}. \tag{62}$$

Let $\mathbf{K}_1'$ be a matrix of size $(n_f{-}1)\times(n_f{-}1)$ that results from eliminating the first column and the first row of $\mathbf{K}_1$. Let $\mathbf{K}_2'$ be a matrix of size $(n_f{-}1)\times(n_g{-}n_f)$that results from eliminating the first row of $\mathbf{K}_2$, and let $\mathbf{K}_3'$ be a matrix of size $(n_g{-}n_f)\times(n_f{-}1)$ that results from eliminating the first column of $\mathbf{K}_3$. In terms of Eqs. (54) and (60) we can obtain

$$\Pi_1 = \left(\frac{\partial\phi}{\partial\mathbf{n}}\right)^{o\mathrm{T}}\mathbf{A}\left(\frac{\partial\phi}{\partial\mathbf{n}}\right)^{o} - \frac{1}{\omega^2}\left(\frac{\partial\phi}{\partial\mathbf{n}}\right)^{o\mathrm{T}}\left(a\mathbf{B}+\frac{T}{\rho}\mathbf{C}\right)\left(\frac{\partial\phi}{\partial\mathbf{n}}\right)^{o}, \tag{63}$$

where

$$\mathbf{A} = (\mathbf{K}'^{+}_{5})^{\mathrm{T}}\mathbf{K}'_1\mathbf{K}^{+}_5 - (\mathbf{K}'^{+}_{5})^{\mathrm{T}}\mathbf{K}'_2\mathbf{K}_6\mathbf{K}'^{+}_{5} - (\mathbf{K}_6\mathbf{K}'^{+}_{5})^{\mathrm{T}}\mathbf{K}'_3\mathbf{K}'^{+}_{5} + (\mathbf{K}_6\mathbf{K}'^{+}_{5})^{\mathrm{T}}\mathbf{K}_4(\mathbf{K}_6\mathbf{K}'^{+}_{5}). \tag{64}$$

Substituting Eq. (63) into Eq. (33), we can obtain the general eigenvalue problem:

$$\left[\mathbf{A} - \frac{1}{\omega^2}\left(a\mathbf{B}+\frac{T}{\rho}\mathbf{C}\right)\right]\left(\frac{\partial\phi}{\partial\mathbf{n}}\right)^{o} = 0. \tag{65}$$

If Eq. (29) is used to apply the pin-end boundary condition, must need eliminate the rows and columns in $\mathbf{A}$, $\mathbf{B}$ and $\mathbf{C}$ that correspond to the nodes at the contact line and obtain the reduced matrices $\mathbf{A}'$, $\mathbf{B}'$ and $\mathbf{C}'$.

Then Eq. (65) is rewritten as

$$\left[\mathbf{A}' - \frac{1}{\omega^2}\left(a\mathbf{B}' + \frac{T}{\rho}\mathbf{C}'\right)\right]\left(\frac{\partial\phi}{\partial\mathbf{n}}\right)^o = 0. \tag{66}$$

If Eq. (35) is used to apply the pin-end boundary condition, a term that denotes the penalty function should be added to the eigenvalue problem (65):

$$\left[\mathbf{A} - \frac{1}{\omega^2}\left(a\mathbf{B} + \frac{T}{\rho}\mathbf{C} + \alpha\mathbf{G}\right)\right]\left(\frac{\partial\phi}{\partial\mathbf{n}}\right)^o = 0. \tag{67}$$

G is a matrix of size $n_f \times n_f$ that results from the dispersion of penalty function. Solving the eigenvalue problem (66) or (67), we can obtain the eigenfrequencies and modes, and the damping rates can be calculated by the formulas in Section 2.2.

3.1.2. Example

Henderson and Miles [5,10] and Carlos Martel et al. [11] studied the surface wave in a brimful circular cylinder with a fixed contact line experimentally and theoretically. The example in their papers will be used to check the computing method above. In this example, as shown in Fig. 3, a circular cylinder container is used, with a radius is 2.766 cm. The liquid is water, and the liquid depth is 3.80 cm. The kinematics viscosity is $0.000001\,\mathrm{m^2\,s^{-1}}$, the surface tension is $0.0724\,\mathrm{N\,m^{-1}}$, and the static contact angle is 90°, so the free surface is flat. The computations here and later were carried out on a computer with a 2.4 GHz Intel Pentium4 processor and 1 Gb of memory.

The experimental, analytical, and numerical values of the frequencies are compared in Table 1, where s is the number of nodal diameters and r the number of nodal circles. A 10-node tetrahedral element is adopted in the computation and the number of elements is 5318. As shown in Table 1, the numerical values are close to

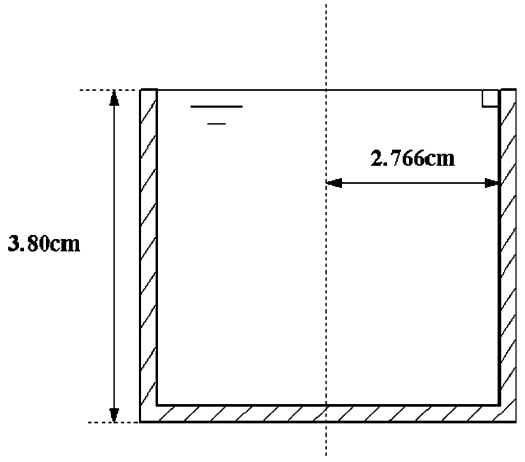

Fig. 3. Sketch map of numerical example with pin-end boundary condition.

Table 1
Experimental, analytical, and numerical values of frequencies of the (s,r) mode with pin-end boundary condition

(s,r)	Frequencies (Hz)				
	(1,0)	(2,0)	(0,1)	(3,0)	(4,0)
Numerical value	4.68	6.35	6.80	7.84	9.29
Analytical value	4.65	6.32	6.84	7.80	9.26
Experimental value	4.69	6.36	6.65	7.94	9.52

Table 2
Frequencies convergence test by number of elements

Number of elements	Frequencies (Hz)		
	(1,0)	(2,0)	(0,1)
48	5.25	7.8	10.5
108	4.89	6.98	7.70
249	4.72	6.57	7.01
450	4.75	6.53	6.88
1375	4.69	6.36	6.74
3167	4.68	6.36	6.77
4086	4.68	6.36	6.79
5318	4.68	6.35	6.80
Analytical value	4.65	6.32	6.84

the analytical and experimental values. As a convergence test for meshing, frequencies corresponding to the first three modes are given in Table 2. As the mesh density increases, the calculated results become closer to the analytical value. Fig. 4 shows the mode shape, which clearly indicates that the contact line is pinned and the contact angle is not always 90° in the case of the pin-end boundary condition. The experimental, analytical and numerical value of damping rates are compared in Table 3. The calculated results and the analytical values are close. Damping ratios corresponding to the first three modes are given in Table 4 as a convergence test for meshing. As shown in Table 4, as the mesh density increases, the calculated results become close to the analytical value in general. But the accuracy does not increase monotonously with mesh density; sometimes the calculated results with a smaller mesh density are better. One possible reason is that the shape of the mesh as well as the density can strongly influence the calculated results of the damping rates.

3.2. Free-end boundary condition

In the case of an irrotational flow and free-end boundary condition there is no dissipation during the sloshing, so Φ and ζ in free oscillation can be expressed by Eqs. (21a, b), too. The equation and boundary conditions that only contain the space variables are Eqs. (25), (26), (27), and (28), and

$$\frac{\partial h}{\partial \mathbf{n}} = 0 \text{ on } L. \tag{68}$$

It has to be pointed out that the $\mathbf{n}$ above is the interior normal at the wall, not at the free surface.

3.2.1. FEM dispersion

The Galerkin statement of the equivalent weak formulation of Eq. (25) and boundary conditions (26), (28), and (68) is

$$\int_\Omega \nabla^2\phi\delta\phi \,\mathrm{d}\Omega - \int_{S_w} \frac{\partial\phi}{\partial\mathbf{n}}\delta\phi \,\mathrm{d}S - \int_{S_f}\left(\left(\frac{a}{\cos\theta} - \frac{T}{\rho}\nabla^2\right)h - \omega\phi\right)\delta h \,\mathrm{d}S - \frac{T}{\rho}\int_L \frac{\partial h}{\partial\mathbf{n}}\delta h \,\mathrm{d}L = 0. \tag{69}$$

Substituting Eq. (31) and (32) into Eq. (69) and using Eq. (27), we can obtain the variational formulation

$$\delta\Pi_3 = 0, \tag{70}$$

where

$$\Pi_3 = \int_\Omega \nabla\phi\nabla\phi \,\mathrm{d}\Omega - \int_{S_f}\frac{a}{\cos\theta}h^2 \,\mathrm{d}S - \int_{S_f}\frac{T}{\rho}\nabla h\nabla h \,\mathrm{d}S. \tag{71}$$

The expressions of Π_1 and Π_3 are the same. The free-end boundary condition (68) is a natural boundary condition and has been contained in Eq. (69), so unlike the pin-end boundary condition, it does not need to be introduced into the variational formulation. After the same course of dispersion in Section 3.1 we can obtain

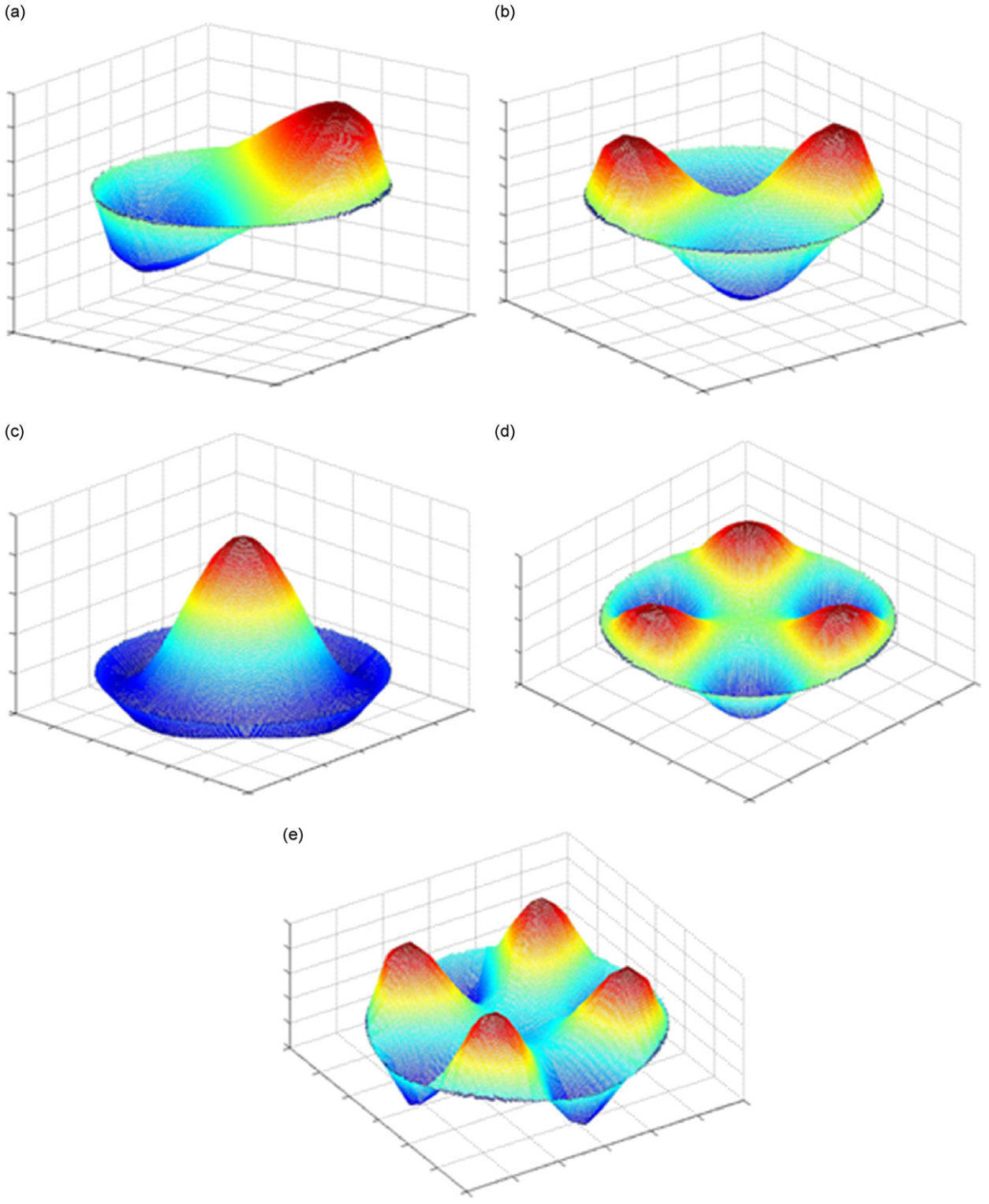

Fig. 4. Sloshing mode shapes in a cylindrical container with pin-end boundary condition: (a) (1,0); (b) (2,0); (c) (0,1); (d) (3,0); and (e) (4,0).

Table 3
Experimental, analytical, and numerical values of damping ratios of the (s,r) mode with pin-end boundary condition

(s,r)	Damping ratios (Hz)				
	(1,0)	(2,0)	(0,1)	(3,0)	(4,0)
Numerical value	3.11×10^{-3}	3.40×10^{-3}	1.83×10^{-3}	3.62×10^{-3}	3.87×10^{-3}
Analytical value	3.17×10^{-3}	3.45×10^{-3}	1.80×10^{-3}	3.72×10^{-3}	4.01×10^{-3}
Experimental value	3.3×10^{-3}	3.6×10^{-3}	2.4×10^{-3}	4.0×10^{-3}	4.0×10^{-3}

Table 4
Damping ratios convergence test by number of elements

Number of elements	Damping ratios (Hz)		
	(1,0)	(2,0)	(0,1)
48	4.77×10^{-3}	4.74×10^{-3}	3.42×10^{-3}
108	3.28×10^{-3}	3.54×10^{-3}	2.28×10^{-3}
249	3.04×10^{-3}	3.34×10^{-3}	1.95×10^{-3}
450	3.24×10^{-3}	3.54×10^{-3}	2.10×10^{-3}
1375	3.07×10^{-3}	3.32×10^{-3}	1.93×10^{-3}
3167	3.08×10^{-3}	3.35×10^{-3}	1.87×10^{-3}
4086	3.10×10^{-3}	3.37×10^{-3}	1.83×10^{-3}
5318	3.11×10^{-3}	3.40×10^{-3}	1.83×10^{-3}
Analytical value	3.17×10^{-3}	3.45×10^{-3}	1.80×10^{-3}

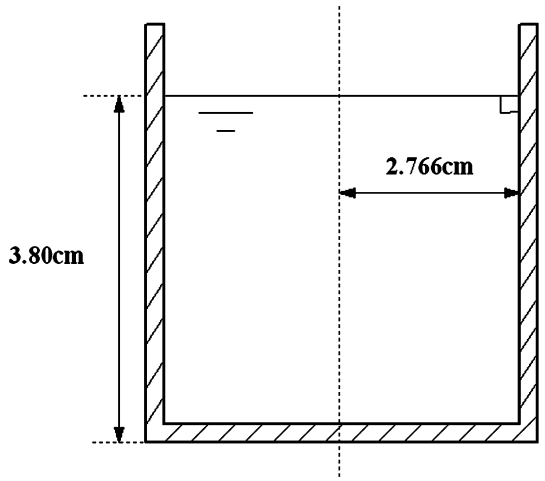

Fig. 5. Sketch map of numerical example with free-end and wetting boundary condition.

the general eigenvalue problem (65). Solving it, we can get the eigenfrequencies and modes, and the damping rates can be calculated by the formulas in Section 2.2.

3.2.2. Example

An example will be given. When the contact angle is 90° and the free surface is flat, the analytical solution for eigenfrequencies and modes of liquid small amplitude sloshing in a cylindrical container with free-end boundary condition is given in Ref. [12]. But in practice the 90° contact angle and the free-end condition cannot be obtained exactly, so there is no experimental value of this case, and the calculated result will be

Table 5
Numerical and analytical values of frequencies of the (s,r) mode with free-end boundary condition

(s,r)	Frequencies (Hz)				
	(1,0)	(2,0)	(0,1)	(3,0)	(4,0)
Numerical value	4.11	5.47	6.26	6.65	7.80
Analytical solution	4.11	5.47	6.25	6.65	7.82

Table 6
Frequencies convergence test by number of elements

Number of elements	Frequencies (Hz)		
	(1,0)	(2,0)	(0,1)
48	4.15	5.68	7.31
108	4.13	5.63	6.75
249	4.08	5.50	6.39
450	4.10	5.50	6.39
1375	4.10	5.45	6.28
3167	4.10	5.46	6.27
4086	4.10	5.46	6.27
5318	4.11	5.47	6.26
Analytical solution	4.11	5.47	6.25

compared only with the analytical solution. As shown in Fig. 5, the radius of the container is 0.02766 m, water is used as the liquid, the liquid depth is 0.038 m, the kinematic viscosity is $0.000001\,\mathrm{m^2\,s^{-1}}$, the surface tension is $0.0724\,\mathrm{N\,m^{-1}}$, and the static contact angle is 90°. A 10-node tetrahedral element is adopted in the computation, and the number of elements is 5318. The numerical and analytical values of frequencies are compared in Table 5. The numerical values are close to the analytical values. Frequencies corresponding to the first three modes are given in Table 6 as a convergence test for meshing. As the mesh density increases, the calculated results become close to the analytical values. Fig. 6 shows the mode shape. It shows that the contact line is removable and the contact angle is always 90° in the case of free-end boundary condition. The analytical and numerical values of damping rates are compared in Table 7. The calculated results and the analytical values are close. As a convergence test for meshing, damping ratios corresponding to the first three modes are given in Table 8. As the mesh density increases, the calculated results become close to the analytical value in general. However, as was the case for the pin-end boundary condition, the accuracy does not increase monotonously with mesh density; sometimes the calculated results with smaller mesh density are better. One possible reason is that the shape of the mesh as well as the density can strongly influence the calculated result of damping rates.

3.3. Wetting boundary condition

In the case of an irrotational flow and wetting boundary condition, if $\lambda \neq 0$ and $\lambda \neq \infty$, there is dissipation at the contact line during sloshing, so Φ and ζ in free oscillation can be expressed as

$$\Phi = \phi\, e^{\omega_1 t} \tag{72a}$$

$$\zeta = h\, e^{\omega_1 t + \psi_1}, \tag{72b}$$

where ω_1 is a complex number whose imaginary part denotes frequency and real part denotes damping, and ψ_1 is a purely imaginary number that denotes the phase difference between Φ and ζ. Substituting Eq. (72) into

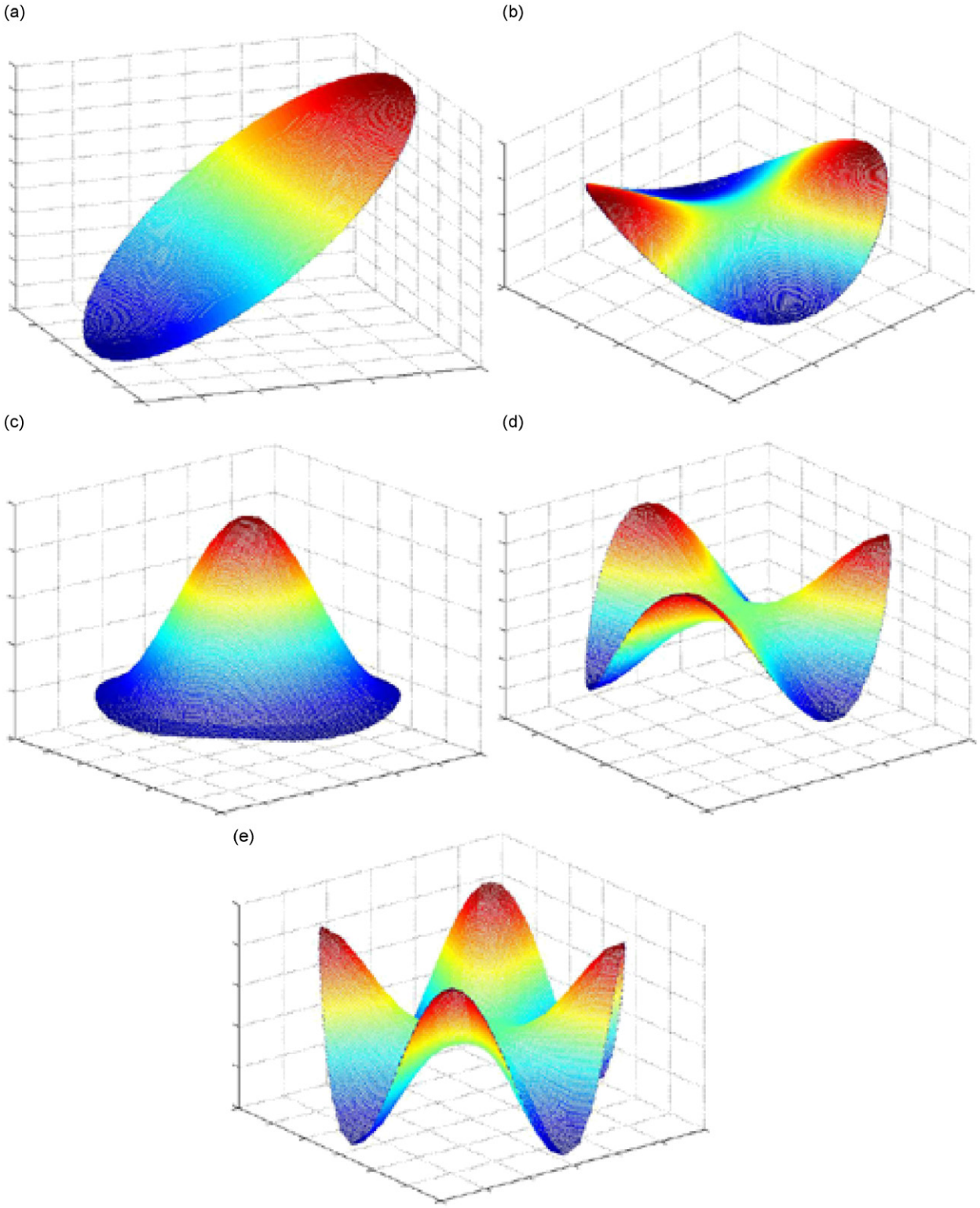

Fig. 6. Sloshing mode shapes in a cylindrical container with free-end boundary condition: (a) (1,0); (b) (2,0); (c) (0,1); (d) (3,0); and (e) (4,0).

Table 7
Numerical and analytical values of damping ratios of the (*s*,*m*) mode with free-end boundary condition

(*s*,*m*)	Damping ratios (Hz)				
	(1,0)	(2,0)	(0,1)	(3,0)	(4,0)
Numerical value	4.90×10^{-3}	6.11×10^{-3}	3.01×10^{-3}	7.15×10^{-3}	7.69×10^{-3}
Analytical solution	4.90×10^{-3}	6.10×10^{-3}	2.95×10^{-3}	7.08×10^{-3}	7.85×10^{-3}

Table 8
Damping ratios convergence test by number of elements

Number of elements	Damping ratios (Hz)		
	(1,0)	(2,0)	(0,1)
48	7.82×10^{-3}	1.08×10^{-2}	7.62×10^{-3}
108	5.09×10^{-3}	6.18×10^{-3}	3.47×10^{-3}
249	4.95×10^{-3}	6.31×10^{-3}	3.32×10^{-3}
450	5.20×10^{-3}	6.17×10^{-3}	3.07×10^{-3}
1375	4.91×10^{-3}	6.16×10^{-3}	3.03×10^{-3}
3167	4.90×10^{-3}	6.12×10^{-3}	3.02×10^{-3}
4086	4.90×10^{-3}	6.14×10^{-3}	3.04×10^{-3}
5318	4.90×10^{-3}	6.11×10^{-3}	3.01×10^{-3}
Analytical solution	4.90×10^{-3}	6.10×10^{-3}	2.95×10^{-3}

Eq. (5), we can obtain

$$\frac{\partial\phi}{\partial\mathbf{n}} = \omega_1 \mathrm{e}^{\psi_1} h. \tag{73}$$

In order to make the equation above valid, ψ_1 must have the form of

$$\psi_1 = \mathrm{i}(k\pi - \varphi'), \tag{74}$$

where

$$\psi' = \arccos\left(\frac{\mathrm{Re}(\omega_1)}{\sqrt{\mathrm{Re}(\omega_1)^2 + \mathrm{Im}(\omega_1)^2}}\right). \tag{75}$$

Let $\psi_1 = \mathrm{i}(\pi/2-\psi')$. Substituting Eq. (72) into Eqs. (2), (3), (4), (5), and (8), we can obtain the equation and boundary conditions that only contain the space variable:

$$\nabla^2\phi = 0 \text{ in } \Omega, \tag{76}$$

$$\frac{\partial\phi}{\partial\mathbf{n}} = 0 \text{ on } S_w, \tag{77}$$

$$\frac{\partial\phi}{\partial\mathbf{n}} = \omega_1 h \mathrm{e}^{\psi_1} \text{ on } S_f, \tag{78}$$

$$\omega_1\phi - \mathrm{e}^{\psi_1}\left(\frac{a}{\cos\theta} - \frac{T}{\rho}\nabla^2\right)h = 0 \text{ on } S_f, \tag{79}$$

$$\omega_1 h = \lambda\frac{\partial h}{\partial\mathbf{n}} \text{ on } L. \tag{80}$$

3.3.1. FEM dispersion

The Galerkin statement of the equivalent weak formulation of Eq. (76) and boundary conditions (77), (79), and (80) is

$$\int_{\Omega} \nabla^2\phi\delta\phi \,\mathrm{d}\Omega - \int_{S_w} \frac{\partial\phi}{\partial\mathbf{n}}\delta\phi \,\mathrm{d}S - \mathrm{e}^{\psi_1}\int_{S_f}\left(\mathrm{e}^{\psi_1}\left(\frac{a}{\cos\theta}-\frac{T}{\rho}\nabla^2\right)h-\omega_1\phi\right)\delta h \,\mathrm{d}S + \frac{\mathrm{e}^{2\psi_1}T}{\rho\lambda}\int_L\left(\omega_1 h-\lambda\frac{\partial h}{\partial n}\right)\delta h \,\mathrm{d}L = 0. \tag{81}$$

Substituting Eqs. (31) and (32) into Eq. (81) and using Eq. (78), we can obtain the variational formulation

$$\delta\Pi_4 = 0, \tag{82}$$

where

$$\Pi_4 = \int_{\Omega}\nabla\phi\,\nabla\phi\,\mathrm{d}\Omega - \mathrm{e}^{2\psi_1}\int_{S_f}\frac{a}{\cos\theta}h^2\,\mathrm{d}S - \mathrm{e}^{2\psi_1}\int_{S_f}\frac{T}{\rho}\nabla h\cdot\nabla h\,\mathrm{d}S + \mathrm{e}^{2\psi_1}\oint_L\frac{T}{\rho\lambda}\omega_1 h^2\,\mathrm{d}L. \tag{83}$$

Eq. (83) is not convenient to be used in the FEM, because ψ_1 is a function of ω_1. In the case of weakly damped sloshing, $|\mathrm{Re}(\omega_1)/\mathrm{Im}(\omega_1)| \ll 1$, so $\psi' \ll 1$ and $\varphi_1 \approx \pi/2$. Let $\varphi_1 = \pi/2$; then Eq. (83) can be rewritten as

$$\Pi_4 = \int_{\Omega}\nabla\phi\,\nabla\phi\,\mathrm{d}\Omega + \int_{S_f}\frac{a}{\cos\theta}h^2\,\mathrm{d}S + \int_{S_f}\frac{T}{\rho}\nabla h\,\nabla h\,\mathrm{d}S - \oint_L\frac{T}{\rho\lambda}\omega_1 h^2\,\mathrm{d}L. \tag{84}$$

Eq. (84) will be used as the variational formulation of the FEM modal analysis later. The dispersion of the first three items in Eq. (84) is the same as that in Section 3.1, and the dispersion of the last item is as follows. Let every line element have p nodes. In element i, h is expressed as

$$h_i = \sum_{j=1}^{p} h_{ij}P_j, \tag{85}$$

where h_{ij} is the value at node j in line element i, and P_j is basis function of node j. Substituting Eq. (85) into the last item of Eq. (84) we can obtain

$$\oint_L\frac{T}{\rho\lambda}\omega_1 h^2\,\mathrm{d}L \approx \frac{T}{\rho\lambda}\omega_1\sum_i\sum_{j=1}^{p}\sum_{k=1}^{p}h_{ij}\left(\int_{L_i}P_jP_k\,\mathrm{d}L_i\right)h_{ik}, \tag{86}$$

where L_i is the region of line element i. Eq. (86) can be further expressed as

$$\oint_L\frac{T}{\rho\lambda}\omega_1 h^2\,\mathrm{d}L \approx \frac{T}{\rho\lambda}\omega_1\sum_i\mathbf{h}^{i\mathrm{T}}\mathbf{D}^i\mathbf{h}^i, \tag{87}$$

Table 9
Numerical and analytical approximate values of the fundamental complex frequencies with wetting boundary of different λ

$1/\lambda$	Fundamental complex frequencies (Hz)	
	Approximate solution	Numerical value
10^5	4.64i	4.69i
10^3	−0.00722 + 4.64i	−0.00687 + 4.69i
10^2	−0.0710 + 4.63i	−0.0630 + 4.68i
10	−0.257 + 4.30i	−0.268 + 4.46i
1	−0.0399 + 4.11i	−0.0688 + 4.11i
0.1	−0.00401 + 4.11i	−0.00695 + 4.11i
0.01	−0.000401 + 4.11i	−0.000695 + 4.11i
0	4.11i	4.11i

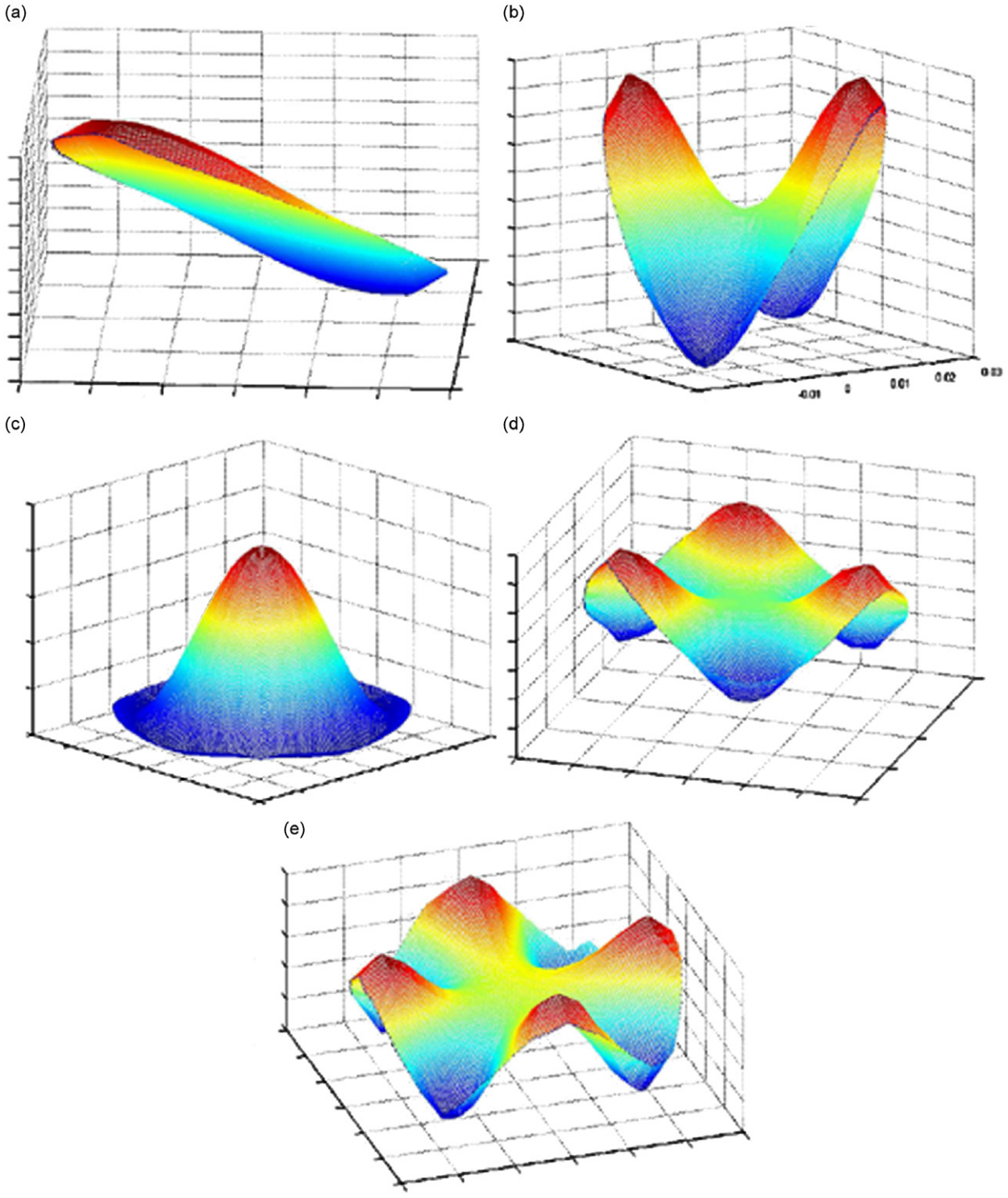

Fig. 7. Sloshing mode shapes in a cylindrical container with wetting boundary condition: (a) (1,0); (b) (2,0); (c) (0,1); (d) (3,0); and (e) (4,0).

where

$$\mathbf{D}^i = \{D^i_{jk}\}, \quad D^i_{jk} = \int_{L_i} \nabla P_j \nabla P_k \, \mathrm{d}L_i, \quad j,k = 1,2,\ldots,p.$$

Arrange values of h at all nodes at the free surface as a column matrix $\mathbf{h}^o$; then

$$\oint_L \frac{T}{\rho\lambda}\omega_1 h^2 \, \mathrm{d}L \approx \frac{T}{\rho\lambda}\omega_1 \mathbf{h}^{o\mathrm{T}}\mathbf{D}\mathbf{h}^o, \tag{88}$$

where $\mathbf{D}$ is a matrix of size $n_f \times n_f$ assembled from $\mathbf{D}^i$. In terms of Eq. (78) the dispersion form of Π_4 is

$$\Pi_4 = \left(\frac{\partial\phi}{\partial\mathbf{n}}\right)^{o\mathrm{T}} \mathbf{A}\left(\frac{\partial\phi}{\partial\mathbf{n}}\right)^{o} + \frac{1}{\omega_1^2}\left(\frac{\partial\phi}{\partial\mathbf{n}}\right)^{o\mathrm{T}}\left(a\mathbf{B} + \frac{T}{\rho}\mathbf{C}\right)\left(\frac{\partial\phi}{\partial\mathbf{n}}\right)^{o} - \frac{T}{\omega_1\rho\lambda}\left(\frac{\partial\phi}{\partial\mathbf{n}}\right)^{o\mathrm{T}}\mathbf{D}\left(\frac{\partial\phi}{\partial\mathbf{n}}\right)^{o}. \tag{89}$$

Substituting Eq. (89) into Eq. (82), we can obtain the quadratic eigenvalue problem:

$$\left[\mathbf{A} - \frac{T}{\omega_1\rho\lambda}\mathbf{D} + \frac{1}{\omega_1^2}\left(a\mathbf{B} + \frac{T}{\rho}\mathbf{C}\right)\right]\left(\frac{\partial\phi}{\partial\mathbf{n}}\right)^{o} = 0. \tag{90}$$

By solving it, we can obtain the complex frequencies ω_1 and modes. The real part of ω_1 denotes the damping caused by dissipation at the contact line. The damping caused by dissipation in the Stokes boundary layer and inner flow can be calculated by the formulas in Section 2.2.

3.3.2. *Example*

Finally, an example is given. The boundary layer approximate solution for complex frequencies of liquid small amplitude sloshing in a cylindrical container with wetting boundary condition is presented in Ref. [9]. The calculated results of the proposed FEM scheme and the approximate solution of a cylindrical container given in Ref. [9] are compared. As shown in Fig. 5, the radius of the container is 0.02766 m, the liquid is water, the liquid depth is 0.038 m, the kinematic viscosity is $0.000001\,\mathrm{m^2\,s^{-1}}$, the surface tension is $0.0724\,\mathrm{N\,m^{-1}}$, and the static contact angle is 90°. A 10-node tetrahedral element is adopted in the computation and the number of elements is 5318. The numerical and analytical approximate values of fundamental complex frequencies corresponding to different λ are compared in Table 9. When $1/\lambda = 0$, it is a free-end boundary condition case, and there is no dissipation at the contact line, so the complex frequency is a purely imaginary number. When $1/\lambda = 10^5$, it is approximate to the case of a pin-end boundary condition; the dissipation at the contact line is very weak, so the real part of the complex frequency is very small and is omitted here. When $1/\lambda$ is equal to other values, the computing result and approximate solution are somewhat different, especially the real part, which denotes damping at the contact line. There are three possible reasons for this. First, the boundary layer approximate solution is not exact itself. Second, in FEM modal analysis the assumption $|\mathrm{Re}(\omega_1)/\mathrm{Im}(\omega_1)| \ll 1$ is adopted and it cannot be met exactly. Third, error is also caused by FEM dispersion. The mode shapes are given in Fig. 7, which shows that the contact line is removable and the contact angle is not always 90° in the case of a wetting boundary condition. Comparing Figs. 4, 6, and 7, it can be found that Fig. 7 is the betweenness of Figs. 4 and 6. There is no analytical formula for the damping of the other parts in a cylindrical container with wetting boundary condition, so the numerical value of damping in the other parts is not shown here.

4. Conclusion

FEMs were established for modal analysis of the liquid small amplitude sloshing with three kinds of contact line boundary conditions. The calculated results are close to the analytical value. When the wetting boundary condition is adopted, the FEM computation makes the assumption that $|\mathrm{Re}(\omega_1)/\mathrm{Im}(\omega_1)| \ll 1$. Sometimes this assumption may not be valid, so how to compute without it is still a problem. In principle, the method in the present paper can be applied to containers of arbitrary shape, but for containers with complex shapes, such as containers with baffles, the effectiveness needs to be studied further.

Acknowledgement

The work described in this paper was supported by the National Natural Science Foundation of China (nos. 10302013 and 10572022).

References

[1] H.N. Abramson, (Ed.), *The Dynamic Behavior of Liquids in Moving Containers*, NASA SP 106, 1966.
[2] T.D. Franklin (Ed.), *The New "Dynamic Behavior of Liquids in Moving Containers"*, Southwest Research Institute, San Antonio, TX, 2002 ⟨http://www.snap.lbl.gov/pub/bscw.cgi/d87835/SwRI_SLOSH_Update.pdf⟩.
[3] T.B. Benjamin, J.C. Scott, Gravity-capillary waves with edge constraints, *Journal of Fluid Mechanics* 92 (1979) 241–267.
[4] J. Graham-Eagle, A new method for calculating eigenvalues with application to gravity-capillary waves with edge constraints, *Mathematical Proceedings of the Cambridge Philosophical Society* 94 (1983) 553–564.
[5] D.M. Henderson, J.W. Miles, Surface-wave damping in a circular cylinder with a fixed contact line, *Journal of Fluid Mechanics* 275 (1994) 285–299.
[6] B. Cocciaro, S. Faetti, C. Festa, Experimental investigation of capillarity effect on surface gravity waves: non-wetting boundary conditions, *Journal of Fluid Mechanics* 246 (1993) 43–65.
[7] L.M. Hocking, The damping of capillary-gravity waves at a rigid boundary, *Journal of Fluid Mechanics* 179 (1987) 253–266.
[8] J.W. Miles, Surface-wave damping in closed basins, *Proceedings of the Royal Society of London A* 297 (1967) 459–475.
[9] J.W. Miles, The capillary boundary layer for standing waves, *Journal of Fluid Mechanics* 222 (1991) 197–205.
[10] J.W. Miles, D.M. Henderson, A note on interior vs. boundary-layer damping of surface waves in a circular cylinder, *Journal of Fluid Mechanics* 364 (1998) 319–323.
[11] C. Martel, J.A. Nicolas, J.M. Vega, Surface-wave damping in a brimful circular cylinder, *Journal of Fluid Mechanics* 360 (1998) 213–228.
[12] K.M. Case, W.C. Parkinson, Damping of surface waves in an incompressible liquid, *Journal of Fluid Mechanics* 2 (1957) 172–184.